NASA TECHNICAL NOTE

NASA TN D-5057

A NUMERICAL METHOD FOR EVALUATION AND UTILIZATION OF SUPERSONIC NACELLE-WING INTERFERENCE

by Robert J. Mack

Langley Research Center
Langley Station, Hampton, Va.

NATIONAL AERONAUTICS AND SPACE ADMINISTRATION • WASHINGTON, D. C. • MARCH 1969

NASA TN D-5057

A NUMERICAL METHOD FOR EVALUATION AND UTILIZATION OF SUPERSONIC NACELLE-WING INTERFERENCE

By Robert J. Mack

Langley Research Center
Langley Station, Hampton, Va.

NATIONAL AERONAUTICS AND SPACE ADMINISTRATION

For sale by the Clearinghouse for Federal Scientific and Technical Information
Springfield, Virginia 22151 – CFSTI price $3.00

A NUMERICAL METHOD FOR EVALUATION AND UTILIZATION OF SUPERSONIC NACELLE-WING INTERFERENCE

By Robert J. Mack
Langley Research Center

SUMMARY

A numerical method for calculating (1) the inviscid flow nacelle-wing interference loads on a warped wing surface, (2) a load-compensating reflex camber surface for optimization purposes, and (3) the interference-lift effective-area contribution to sonic-boom pressure disturbances has been presented and discussed. Within the limitations of a modified supersonic linearized theory, the numerical method can provide reasonable good estimations of the loads imposed on a wing surface by nacelles mounted nearby.

INTRODUCTION

Application of supersonic flow theory to the design and evaluation of aerodynamically efficient supersonic-cruise aircraft has been greatly facilitated by the recent employment of the high-speed digital computer. Simple numerical methods which closely approximate the behavior of complex integral equations can be programed for the computer to give quick solutions to aerodynamic theory problems and can extend greatly the range of problems that may be handled. For example, the program described in reference 1 computes an optimized camber surface at a given Mach number for a wing of arbitrary planform, whereas those of references 2 and 3 determine the aerodynamic characteristics of a given wing with an arbitrary planform and camber surface. The wave drag of an entire configuration may be evaluated with the program outlined in reference 4. Similar unpublished programs based on the Sommer-Short T-prime method permit the calculation of the skin-friction drag of the configuration. With these programs, the overall aerodynamic characteristics of a proposed design can be found with a reasonably good degree of accuracy for most slender-body thin-wing aircraft.

In estimating the overall aerodynamic characteristics of a configuration employing nacelles or stores, a means of evaluating the interference forces is required. The computation technique described in this report provides a method for determining the distribution and intensity of the interference forces on a warped wing surface.

However, airplane design studies which must include nacelle-induced drag minimization require more than a knowledge of the interference forces. Achievement of the highest

possible level of aerodynamic efficiency demands careful consideration of the manner in which the nacelles and the wing are integrated. Current design practice, as discussed in reference 5, is based on the concepts of favorable interference and wing reflexing (warping the wing surface away from the nacelles). Nacelles positioned under the wing trailing edge give, in general, relatively low wave drag. Wing reflexing utilizes the idea that a localized warping of the wing surface will produce an incremental loading opposite of that induced by the nacelles and will give a combined lift and moment loading, due to wing and nacelle, which can be the same as the optimized loading originally designed for the wing. A numerical method for determining reflexed wing coordinates which makes use of the previously discussed nacelle interference loadings and incorporates the wing camber design method of reference 1 is considered in this report.

Also discussed is the effect of the nacelle-wing interference on the flow field under the aircraft. Changes in the airplane lift distribution brought about by the nacelle pressure field acting on the wing surface affect not only the drag, but also the distribution of the pressure in the shock field surrounding the airplane. Thus, the nacelle flow-field computation is also useful in a sonic-boom analysis using the methods discussed in reference 6.

In summary then, these three items are discussed in this report: (1) calculation of the nacelle-wing interference forces, (2) calculation of a reflexed wing camber surface, and (3) calculation of the incremental lift distribution which is used in a sonic-boom analysis. Necessary assumptions are mentioned as they are needed in the discussion and presentation.

Since the object of the present study is to provide a simplified method of accounting for nacelle effects to supplement existing configuration analysis programs, the use of more refined or more rigorous solutions than those employed in the previously mentioned work would seem to be unnecessary. However, the calculation of interference forces and wing reflexing requires that very good approximations to actual pressure disturbance locations be made. The method used in this report utilizes the modified linearized theory developed by G. B. Whitham (ref. 7). It not only overcomes the difficulty of obtaining solutions for ducted nacelles, but also calculates the positions and strengths of shock waves originating at the nose and surface discontinuities of the nacelle or store. Several examples are presented to show comparisons of nacelle pressure fields calculated by the numerical method with those measured in wind-tunnel experiments, and to illustrate practical applications to aircraft design analysis.

SYMBOLS

A	nacelle cross-section area
A(L,N)	interference zone grid element weight factor
b	wing span
B(L,N)	wing area grid element weight factor
c	wing chord
$\bar{c}$	mean geometric chord
C_D	pressure drag coefficient
C_L	lift coefficient
C_m	moment coefficient about $0.25\bar{c}$ based on mean geometric chord
$C_{m,o}$	moment coefficient at $C_L = 0$
C_p	pressure coefficient
ΔC_p	lifting pressure coefficient
F(t)	area distribution function (called F(y) in ref. 7)
h	area influence function (called h(x) in ref. 7)
K	reflex factor, $\frac{\text{Load canceled}}{\text{Load induced}}$
l	maximum length on wing
l_n	nacelle length
L,N	designation of influencing grid elements (see fig. 3)
L^*,N^*	designation of field-point grid elements (see fig. 3)

M	Mach number
x,y,z	distances along Cartesian coordinate axes X, Y, and Z
x,r	distances along cylindrical coordinate axes X,R
t	dummy variable along X-axis, used in F(t) calculation
R	body radius
S	wing area
U_∞	free-stream velocity
$\beta = \sqrt{M^2 - 1}$	
γ	ratio of specific heats, 1.4 for air
ξ,η	dummy variables along x,y directions
Λ	leading-edge sweep angle
ϕ	perturbation potential

Subscripts:

av	average
c	camber surface
e	effective
I	due to interference
max	maximum
min	minimum
si	shock-wave—camber-surface intersection

ℓe leading edge

te trailing edge

n value on nacelle

Primes denote derivatives with respect to length t. The symbol Δ denotes incremental quantities.

THEORY AND DISCUSSION

Interference Force Determination

A simplified representation of the nacelle interference problem is shown in figure 1. The sketch depicts a warped-delta-wing ducted-nacelle configuration in supersonic flow. A fuselage is not shown so that attention can be focused on the nacelle-wing interference. The determination of interference forces on this configuration is made with due regard to the capabilities of other computer programs with which it is to be used concurrently in analysis work. Wave drag due to wing and nacelle thickness (including mutual interference) is accounted for in the wave drag program of reference 4. Therefore, the method of this report is applicable only in the calculation of the lifting forces on the wing resulting from nacelle thickness, and to any drag component that results from the inclination of the wing mean camber surface. The effect on the nacelle of the wing lift-induced pressure field has been neglected since that drag contribution is assumed to be small. Similarly, the effect of the reflection of the nacelle pressure field from the wing surface has been neglected. It might be noted that a wing reflex surface designed to compensate for the nacelle-induced wing loading will reduce or eliminate this latter drag contribution.

Figure 2 shows the nacelle referencing coordinates, and figure 3, the grid element system used to define the wing and its camber surface. This coordinate system is the same as that used to describe the wing in references 1 to 3.

The linearized flow equation for the perturbation potential about a body of revolution in supersonic flow is

$$\beta^2 \frac{\partial^2 \phi}{\partial x^2} - \frac{1}{r} \frac{\partial \phi}{\partial r} - \frac{\partial^2 \phi}{\partial r^2} = 0 \tag{1}$$

Bodies with noncircular cross sections can also be analyzed if the geometry and probable attendant flow field will not be greatly distorted by using one or more bodies of revolution whose total area and area buildup are the same as those of the original (ref. 4).

The classical solution is derived by representing the body by a line of sources and having the pressure disturbances propagate outward along Mach lines. G. B. Whitham modified this solution by replacing the Mach line characteristic

$$x - \beta r = \text{Constant} \tag{2}$$

with a more exact characteristic

$$x - \beta r = t - \frac{(\gamma + 1)M^4}{\sqrt{2\beta^3}}\sqrt{r}\, F(t) \tag{3}$$

where

$$F(t) = \int_0^{\infty} \sqrt{\frac{2}{\beta R(\xi)}}\, h\left(\frac{t - \xi}{\beta R(\xi)}\right)\frac{dA'(\xi)}{2\pi} \tag{4}$$

and t is a constant equal to $x - \beta R(x)$ where the characteristic meets the body surface (eq. (12), ref. 7). This Stieltjes integral form for $F(t)$ is used instead of the "smooth" body form

$$F(t) = \frac{1}{2\pi}\int_0^t \frac{A''(\xi)d\xi}{\sqrt{t - \xi}} \tag{5}$$

because, in general, nacelles do not always have smooth and continuous surface slopes, and the effects of these discontinuities are more noticeable in the flow field near the body which impinges on the wing surface. In the case where the body shape is smooth, and surface slopes are analytically continuous, both forms of $F(t)$ give the same solution.

Ahead of the inlet, the flow is undisturbed by the nacelle; thus a long cylindrical stream tube can be extended forward from the intake without changing the flow characteristics. Along this stream tube, $\Delta A' = 0$; therefore, $F(t) = 0$ for all $t < -\beta R(0)$. This initial point $t = -\beta R(0)$ is the intersection on the body axis of a Mach line from the nacelle lip and corresponds to the point where an abrupt change in source strength would cause a discontinuity in $\Delta A'$ on the stream-tube—nacelle surface. The step change in $F(t)$ due to this flow deflection at the lip is

$$\Delta F(t) = \sqrt{\frac{2}{\beta R(0)}}\,\frac{\Delta A'}{2\pi} \tag{6}$$

which is equation (26) of reference 7. Beyond the lip source point, $t > -\beta R(0)$, values of $F(t)$ are calculated from equation (4) in the form

$$F(t) = \frac{1}{2\pi} \sum \sqrt{\frac{2}{\beta R(\xi)}}\, h\left(\frac{t - \xi}{\beta R(\xi)}\right) \Delta A'(\xi) \tag{7}$$

where a summation operation replaces an integration over a range of ξ starting at $\xi = -\beta R(0)$ and extending to the point on the body surface where a Mach line from t intersects (see fig. 4(a)). The field point distance r and the body radius $R(t)$ determine the slope $\Delta F/\Delta t$ of the lines which change the $F(t)$ curve to a pressure profile through the relationship

$$\frac{\Delta F}{\Delta t} = \frac{\gamma + 1}{\sqrt{2\beta^3}} \frac{M^4}{\sqrt{r} - \sqrt{R(t)}} \tag{8}$$

as seen in figure 4(b) and described in reference 8. Figures 4(a) and 4(b) show the components which make up the $F(t)$ calculation, their relationship to nacelle thickness, nacelle surface slope and Mach number, and that a $\Delta C_{p,I}$ can be found by suitably modifying the $F(t)$ curve. Notice that the approximation

$$\frac{1}{\sqrt{r}} \approx \frac{1}{\sqrt{r} - \sqrt{R(t)}} \tag{9}$$

is very good when r is more than one or two body lengths, and the nacelle or pod is truly "slender."

The calculation of shocks and shock locations from the $F(t)$ curve is explained fully in reference 7, and the computational technique used in the computer program is detailed in reference 8. The value of $\Delta C_{p,I}$ is found from a first-order truncation of the series expansion for C_p in a perturbated flow field which is doubled to account for pressure wave reflection from wing surface (refs. 6 and 8). When only parts of the field where no shocks are present are considered, $\Delta C_{p,I}$ is simply

$$\Delta C_{p,I} = \sqrt{\frac{8}{\beta r}}\, F(t) \tag{10}$$

and is calculated at the trailing edge of each grid element block within the zone of nacelle-wing interference. This interference zone is the area bounded by the intersection of the shock surface from the lip of the nacelle (no duct flow spillage being assumed) or the nose of the pod (an attached shock being assumed) and the wing camber surface. Appreciable interference force error can occur if portions of the interference zone extend forward of the leading edge or outward of the wing tip and the disturbance field can spill

over onto the upper surface. In such cases, the field point pressure is influenced by both the camber surface and the nacelle within the forward-facing characteristic surface, and cannot be calculated by the method outlined in this report.

A mean $\Delta C_{p,I}$ over each grid element area is found from

$$\Delta C_{p,I}(L^*,N^*)_{av} = \frac{\left[\Delta C_{p,I}(L^* - 1,N^*) + \Delta C_{p,I}(L^*,N^*)\right]}{2}$$

Outside the interference zone, $\Delta C_{p,I}(L^*,N^*)_{av} = 0$. Overall values of interference lift and drag are obtained from

$$C_L = \frac{\sum_{L=1}^{L_{max}} \sum_{N_{min}}^{N_{max}} \Delta C_{p,I}(L^*,N^*)_{av}\, A(L^*,N^*)}{\beta S}$$

$$C_D = \frac{\sum_{L=1}^{L_{max}} \sum_{N_{min}}^{N_{max}} \Delta C_{p,I}(L^*,N^*)_{av}\, A(L^*,N^*) \frac{\partial z}{\partial x}(L^*,N^*)}{\beta S}$$

$$S = \frac{\sum_{L=1}^{L_{max}} \sum_{N_{min}}^{N_{max}} B(L^*,N^*)}{\beta}$$

The weight factors $A(L^*,N^*)$ and $B(L^*,N^*)$ are determined from the conditions

$$A(L^*,N^*) = 0 \qquad \left(L^* - x_{si} \leqq 0\right)$$

$$A(L^*,N^*) = L^* - x_{si} \qquad \left(0 < L^* - x_{si} < 1\right)$$

$$A(L^*,N^*) = 1 \qquad \left(L^* - x_{si} \geqq 1\right)$$

$$B(L^*,N^*) = 0 \qquad \left(L^* - x_{le} \leqq 0;\ \ L^* - x_{te} \geqq 1\right)$$

$$B(L^*,N^*) = L^* - x_{le} \qquad \left(0 < L^* - x_{le} < 1\right)$$

$$B(L^*,N^*) = 1 - \left(L^* - x_{te}\right) \qquad \left(0 < L^* - x_{te} < 1\right)$$

$$B(L^*,N^*) = 1 \qquad \left(L^* - x_{le} \geqq 1;\ \ L^* - x_{te} \leqq 0\right)$$

Reflex Camber Surface Determination

A method for computing a camber surface for a specified loading is outlined in reference 1 and is based on the equations

$$\frac{\partial z}{\partial x}(x,y) = -\frac{\beta}{4}\Delta C_p(x,y) + \frac{1}{4\pi}\iint \frac{(x - \xi)\,\Delta C_p(\xi,\eta)\,d\xi\,d\eta}{(y - \eta)^2\sqrt{(x - \xi)^2 - \beta^2(y - \eta)^2}} \tag{11}$$

$$z_c(x,y) = \int \frac{\partial z}{\partial x}(x,y)\,dx \tag{12}$$

where $\Delta C_p(x,y)$ and $\Delta C_p(\xi,\eta)$ are the incremental lifting pressures on the wing camber surface. These equations are suitably modified to fit the grid-element coordinate system shown in figure 3, and adapted for a numerical solution on the digital computer.

By changing the sign of $\Delta C_p(x,y)$ and $\Delta C_p(\xi,\eta)$ and using them to represent the nacelle interference pressure field, the equations and method can be used to generate a reflex surface which will cancel all or a part of the initial interference lift. New force characteristics are then determined by computing the interference lift and drag on the reflexed camber surface. The required force condition is

$$\left[C_{L,c} + (1 - K)C_{L,I}\right]_{\text{unreflexed wing}} = \left(C_{L,c} + C_{L,I}\right)_{\text{reflexed wing}} \tag{13}$$

that is, the sum of the wing camber lift and the nacelle-wing interference lift minus the amount of interference lift to be canceled on the initial wing surface is equal to the camber lift plus the interference lift on the reflexed wing surface. A second constraint is that the moment change on the unreflexed wing must be equal to that induced on the reflexed wing. An iteration method is used to find a solution which satisfies the lift and moment constraints.

The necessity for using both of these requirements can be illustrated by considering the 100-percent reflex case. With all the initial interference lift canceled, the $C_{m,o}$ and the total lift of the nacelle-wing combination at zero angle of attack must be the same as those of the unreflexed wing alone at the same attitude so that the initial optimized lift and moment loading can be assumed to have been restored.

Sonic-Boom Effective-Area Contribution

Part of the interference lift computation consists of determining what percentage has been developed at stations along the X-axis. It is this accumulated lift that determines the interference lift contribution to the sonic-boom pressure field directly below the airplane. The sonic-boom program requires area distributions which are composed of volume and lift components superimposed at their proper locations along the aircraft reference line. Interference lift contributes an effective area defined by

$$A_e(x) = \frac{\beta}{2} C_L(x)\, S \tag{14}$$

where $C_L(x)$ is the portion of the total interference lift that has accumulated at the length x.

EXAMPLES

Interference Pressure Determination

A simplified ducted body (fig. 5) was used to compare numerical and experimental values of free stream C_p at a free-stream Mach number of 2.96. The truncated-cone forebody had a lip angle $\left(\tan^{-1}\frac{dr}{dx} \text{ at } x = 0\right)$ of about 3.61° and was 1.75 inches (4.445 cm) long. A 2.25-inch (5.715-cm) cylindrical aft section completed the model which although a bit stubby, was still a reasonably good nacelle representation.

The results of wind-tunnel tests and numerical-method calculations are shown for comparison in figure 5 for two distances measured in terms of nacelle body length. A similar comparison for a slender cone-cylinder body at $M = 2.0$ is shown in figure 5 of reference 6. In both cases, the numerical solution gives a good estimate of the pressure signature. The rounding of the nose shock in the ducted nacelle case is due to tunnel turbulence, model vibration, probe vibration, and probe boundary layer.

Figures 6(a) and 6(b) show convergence results for a similar truncated-cone, cylindrical afterbody, ducted nacelle located under a rectangular flat plate in $M = 2$ flow. For this case which is typical of many design situations, a satisfactory prediction is achieved with the use of 20 or more elements along the semispan and 16 or more body stations. There is some uncertainty in fixing the minimum number of body stations, however, due to the nonuniformity of the wing-intercepted flow field. Both positive and negative C_p regions occur, and the change in C_p across the shoulder is very pronounced. A sufficient number of $F(t)$ points (corresponding to the number of body stations) must be available to define the shoulder expansion and recompression pressures

at intervals compatible with the grid element size, or the estimates of lift, drag, and moment will have significant errors.

Interference and Reflex Determination

A wing-nacelle arrangement (fig. 7) was studied to determine the effect of nacelle interference and camber-surface reflexing on performance. The wing was a delta planform of $\beta \cot \Lambda = 0.5$ whose surface was twisted and cambered to provide minimum drag due to lift at $M = 2.0$ for a design C_L of 0.1. Two bodies of revolution composed of a truncated-cone forebody and a cylindrical aft section represented the ducted nacelles. The forebody had a length of $0.1875l$, a minimum diameter of $0.0344l$, and a maximum diameter of $0.0625l$, whereas the cylindrical aft section had a length of $0.094l$.

Figure 8 shows the effect of nacelle interference on the optimum camber surface drag polar when no reflexing is present. The addition of nacelles to the optimized camber shape resulted in a negligible improvement to the drag characteristics at design C_L, but did increase the nosedown pitching moment, as was expected. There may be some question concerning the addition of an arbitrary loading (due to nacelle interference) to a presumed optimum wing loading to obtain a further drag reduction. However, it must be remembered that the nacelle is an external element not included in the original wing design problem. In effect, a new optimizing problem is created and an important question is raised: In this new situation, will the restoration of the optimum wing loading, or some other loading, result in further benefits?

Varying the amount of reflexing gave a small but noticeable improvement in drag at $C_L = 0.1$ for relatively small departures from the original optimized camber surface (fig. 9). A quantitative analysis to establish a level of reflexing for minimum C_D at design C_L is outside the scope of this report. Figure 9 is included to demonstrate that the computer program could be useful in such a study.

In figure 10, three schematic sketches show, by using the right-hand side only, the nacelle-wing configuration, the induced pressure field, and the resultant reflexed camber surface in a somewhat exaggerated scale. Although the interference pressures start abruptly and change markedly across the chord, the reflex surface varies smoothly and gradually, a slope discontinuity occurring only at the border of the interference region. The small differences between the original and the reflexed camber can be seen on the sketch to the right of the reflexed wing surface drawing. However, the gradual changes in slope and height of this reflex surface do not remove the need for the designer to exercise discretion and judgment, based on practical experience, in positioning the nacelles and selecting the amount of interference lift cancellation.

The final example (fig. 11) shows how the method is used to provide inputs to a sonic-boom analysis of an aircraft configuration. A simple, ducted, parabolic body was placed below a flat-plate representation of a wing. The curves described the pressure disturbances due to nacelle interference felt directly below the aircraft in terms of an effective area ratio. With the nacelle below the wing, the effect is almost double that of the nacelle volume taken by itself. Nonlinear behavior of the Whitham flow equations causes the ratio of the effective area due to lift to the maximum body area to exceed 1.0. The relatively small amount of residual effective area that remains beyond the wing trailing edge or the body end point is the result of small errors in the numerical calculations and of cutting off the solution at twice the body length instead of at infinity. These errors would be inconsequential in the total sonic-boom analysis.

CONCLUDING REMARKS

A numerical method for calculating (1) the inviscid flow, nacelle-wing interference loads on a warped wing surface, (2) a load-compensating reflex camber surface for optimization purposes, and (3) the interference-lift effective area contribution to sonic-boom pressure disturbances has been presented and discussed. Within the limitations of a modified supersonic linearized theory, the numerical method can provide reasonably good estimations of the loads imposed on a wing surface by nacelles mounted nearby.

Langley Research Center,
National Aeronautics and Space Administration,
Langley Station, Hampton, Va., November 26, 1968,
126-13-02-08-23.

REFERENCES

1. Carlson, Harry W.; and Middleton, Wilbur D.: A Numerical Method for the Design of Camber Surfaces of Supersonic Wings With Arbitrary Planforms. NASA TN D-2341, 1964.

2. Middleton, Wilbur D.; and Carlson, Harry W.: Numerical Method of Estimating and Optimizing Supersonic Aerodynamic Characteristics of Arbitrary Planform Wings. J. Aircraft, vol. 2, no. 4, July-Aug. 1965, pp. 261-265.

3. Middleton, Wilbur D.; and Carlson, Harry W.: A Numerical Method for Calculating the Flat-Plate Pressure Distributions on Supersonic Wings of Arbitrary Planform. NASA TN D-2570, 1965.

4. Harris, Roy V., Jr.: An Analysis and Correlation of Aircraft Wave Drag. NASA TM X-947, 1964.

5. Robins, A. Warner; Morris, Odell A.; and Harris, Roy V., Jr.: Recent Research Results in the Aerodynamics of Supersonic Vehicles. J. Aircraft, vol. 3, no. 6, Nov.-Dec. 1966, pp. 573-577.

6. Carlson, Harry W.; Mack, Robert J.; Morris, Odell A.: Sonic-Boom Pressure-Field Estimation Techniques. J. Acoust. Soc. Amer., vol. 39, no. 5, pt. 2, May 1966, pp. 510-518.

7. Whitham, G. B.: The Flow Pattern of a Supersonic Projectile. Commun. Pure Appl. Math., vol. V, no. 3, Aug. 1952, pp. 301-348.

8. Middleton, Wilbur D.; and Carlson, Harry W.: A Numerical Method For Calculating Near-Field Sonic-Boom Pressure Signatures. NASA TN D-3082, 1965.

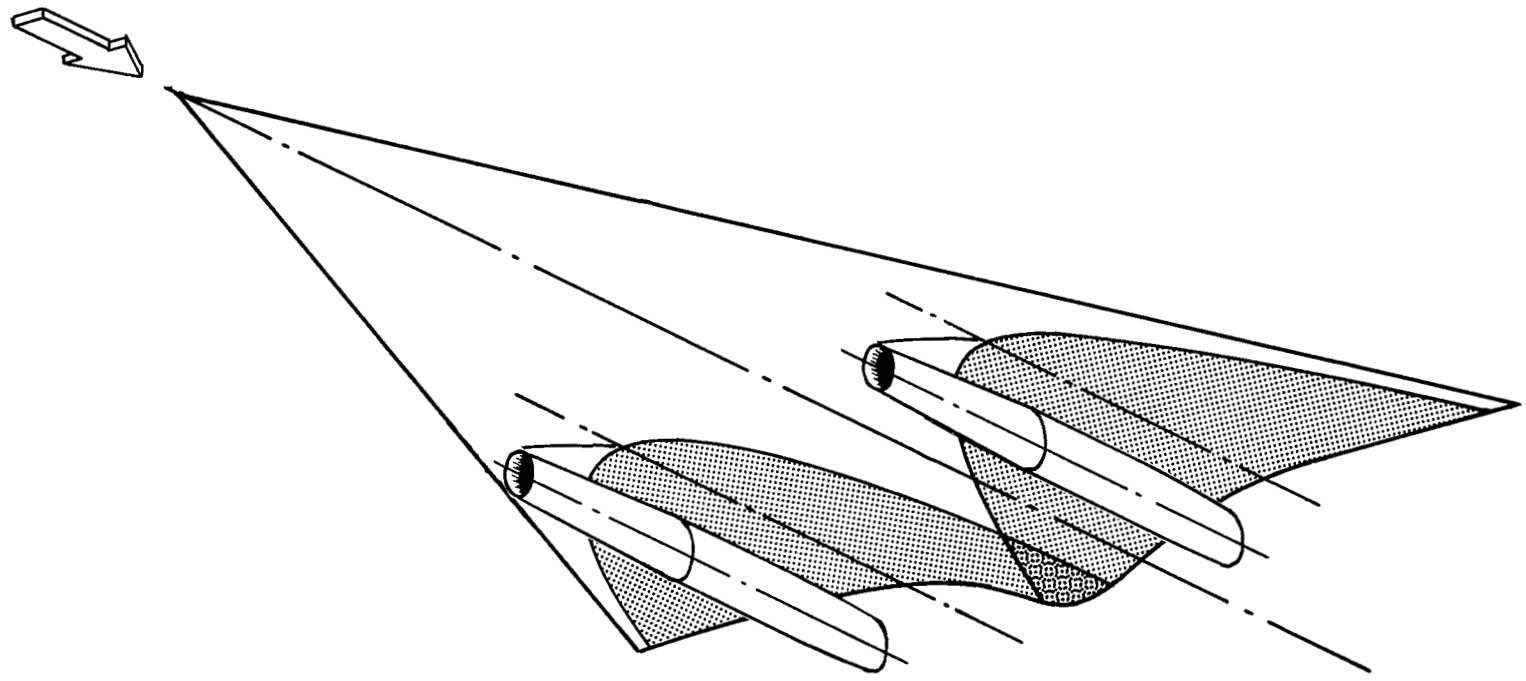

Figure 1.- Pictorial representation of nacelle-wing interference problem. Shaded area indicates interference region.

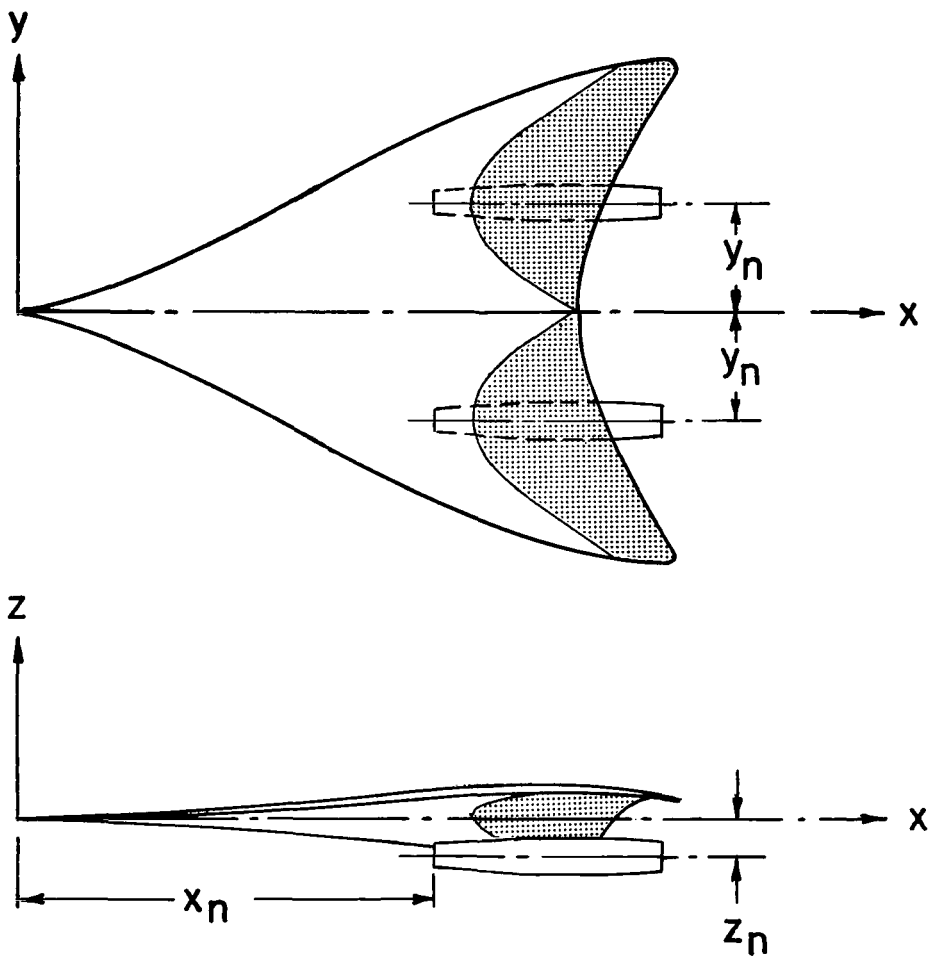

Figure 2.- Coordinate system used in analysis of nacelle-wing interference. Shaded area indicates interference region.

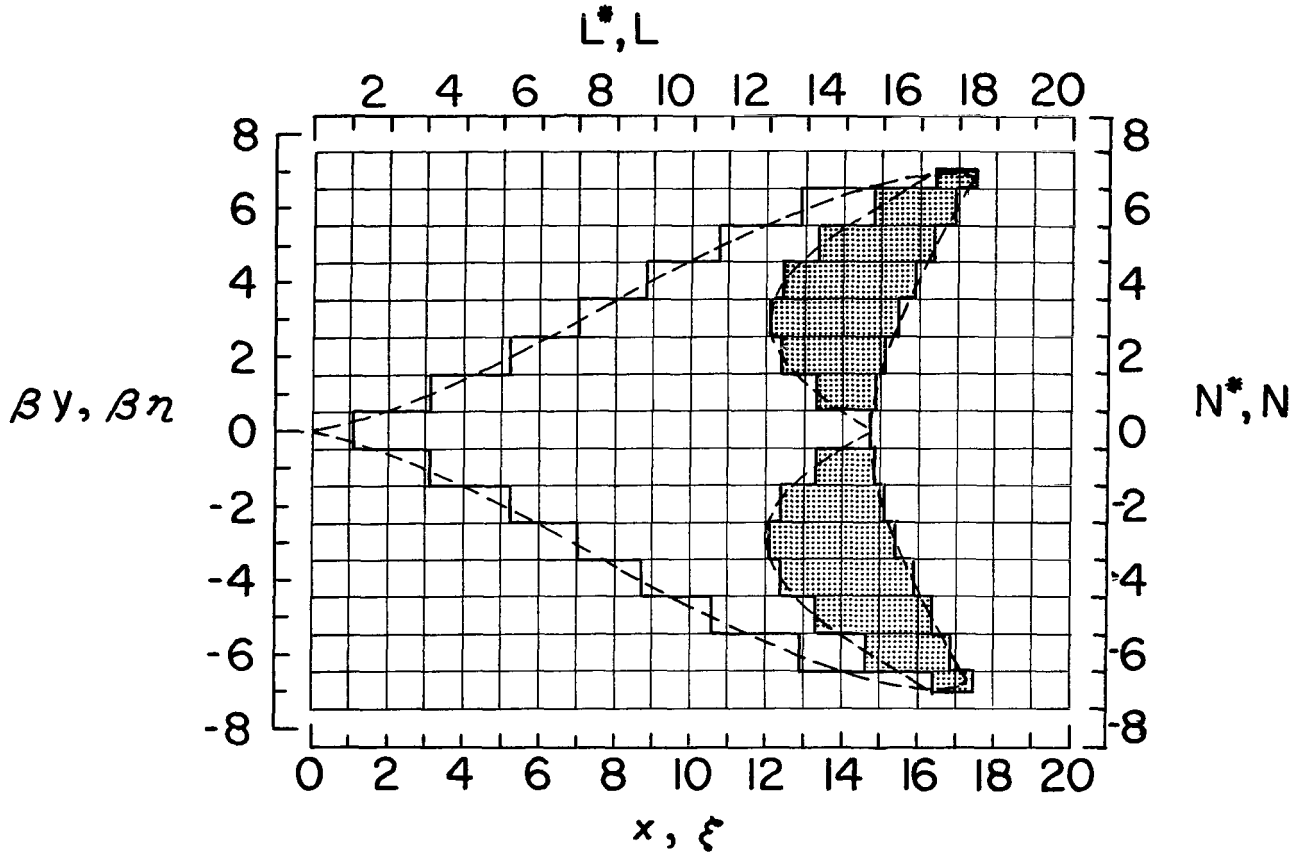

Figure 3.- Grid system used to represent wing surface. Shaded area indicates interference region.

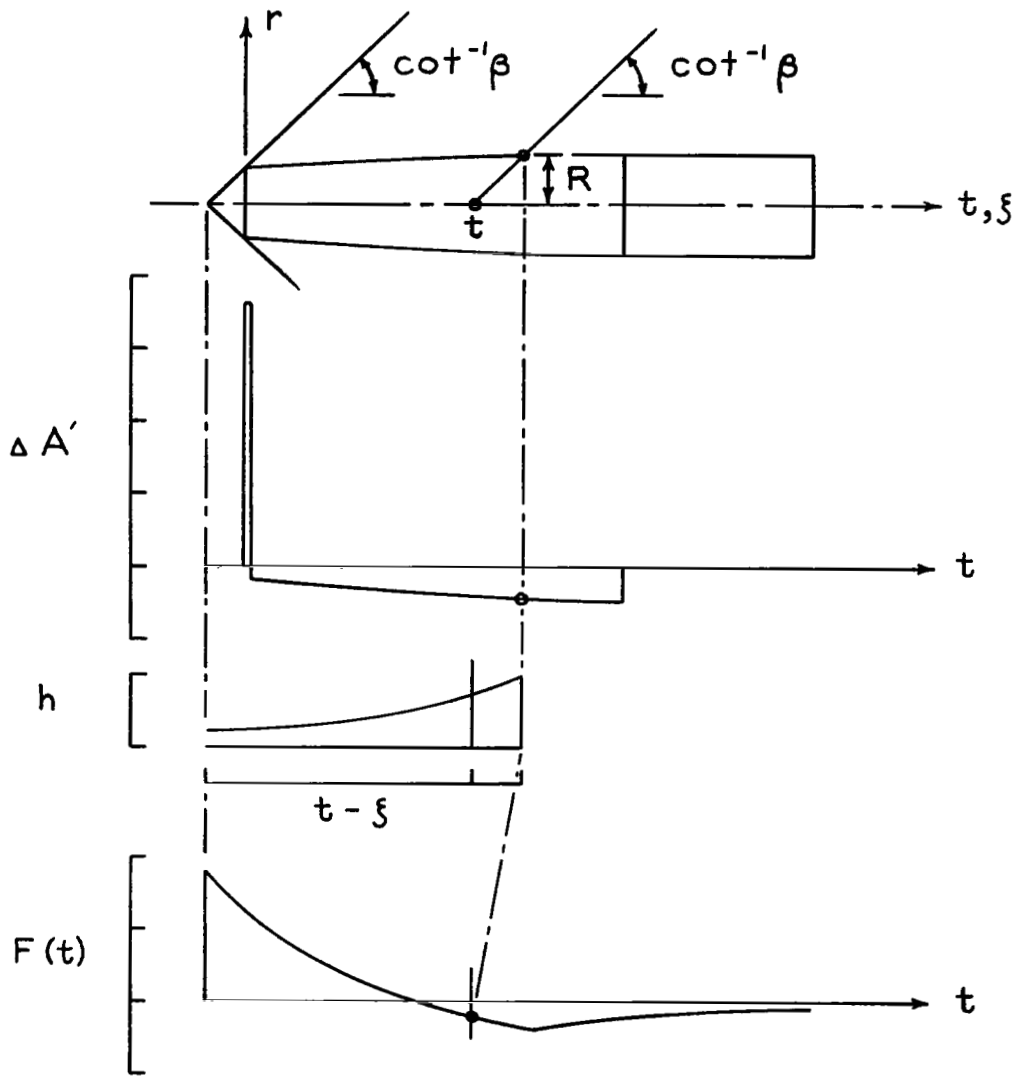

(a) Components of F-function.

Figure 4.- Graphical presentation of parameters in nacelle flow-field solution.

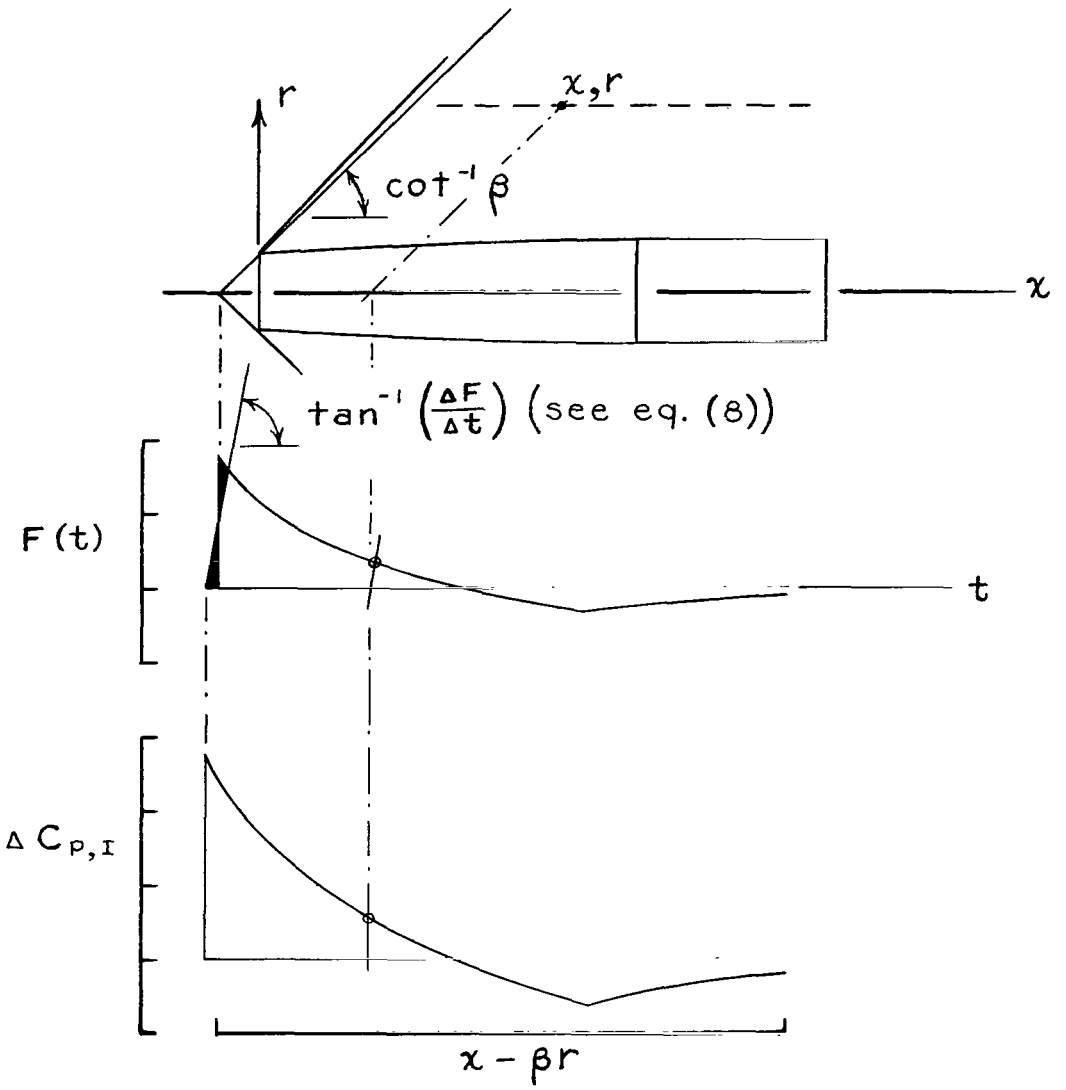

(b) F-function modification to obtain field pressures.

Figure 4.- Concluded.

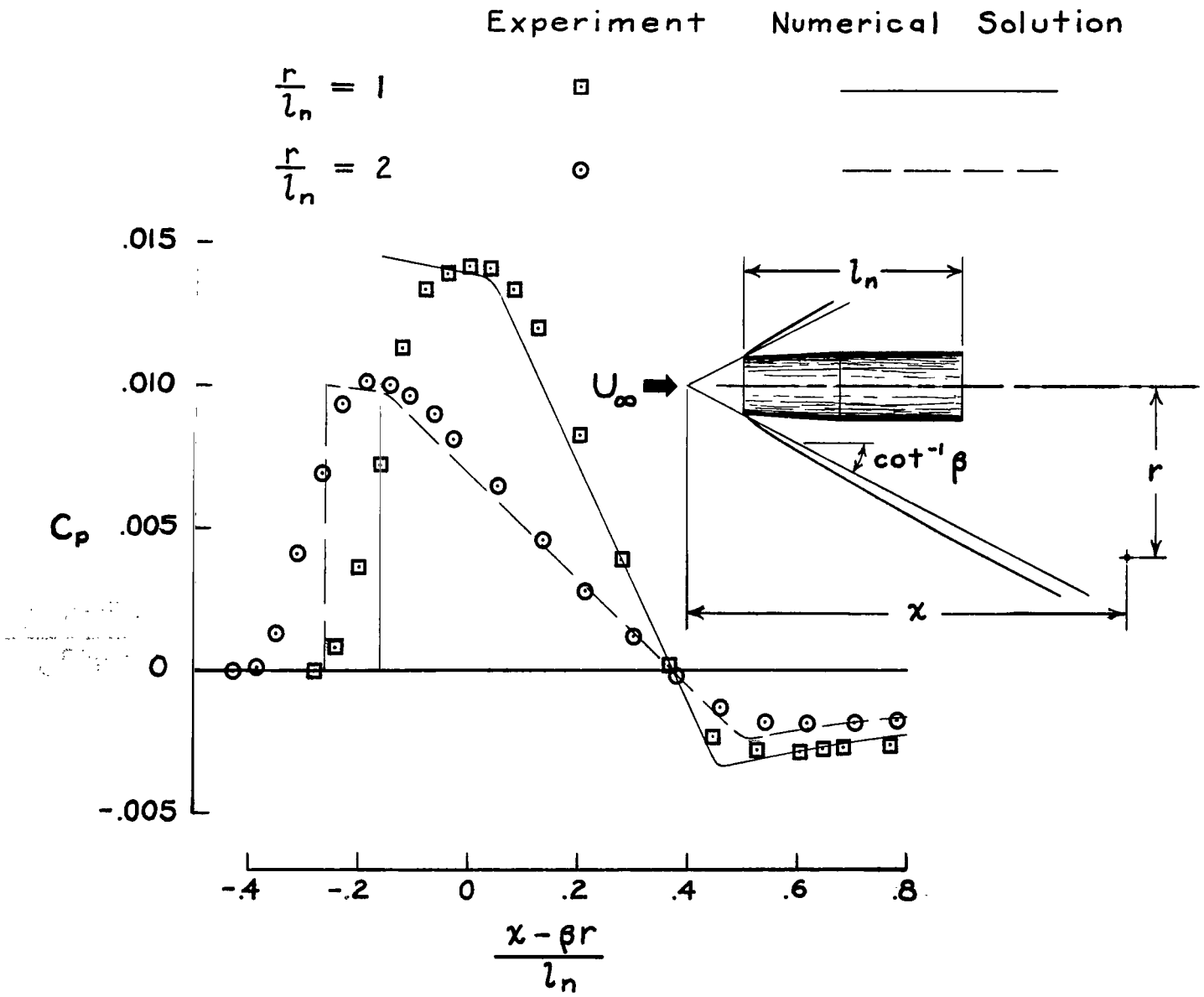

Figure 5.- Comparison of experimental and numerical solution for a ducted nacelle at M = 2.96.

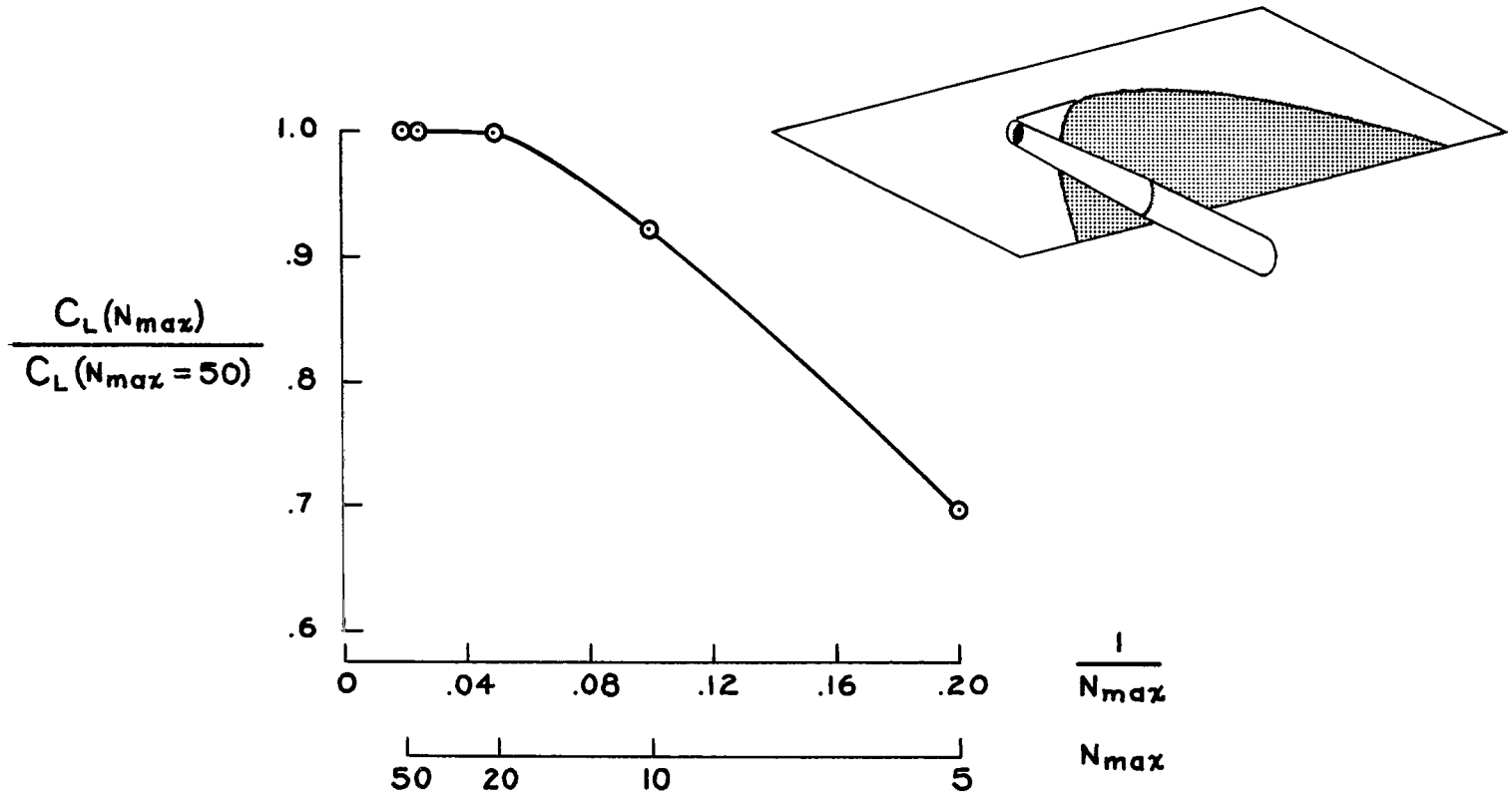

(a) $\frac{\Delta l_n}{l_n} = 0.011$, M = 2.0.

Figure 6.- Lift-coefficient convergence for a ducted nacelle and a flat streamwise plate. Shaded area indicates interference region.

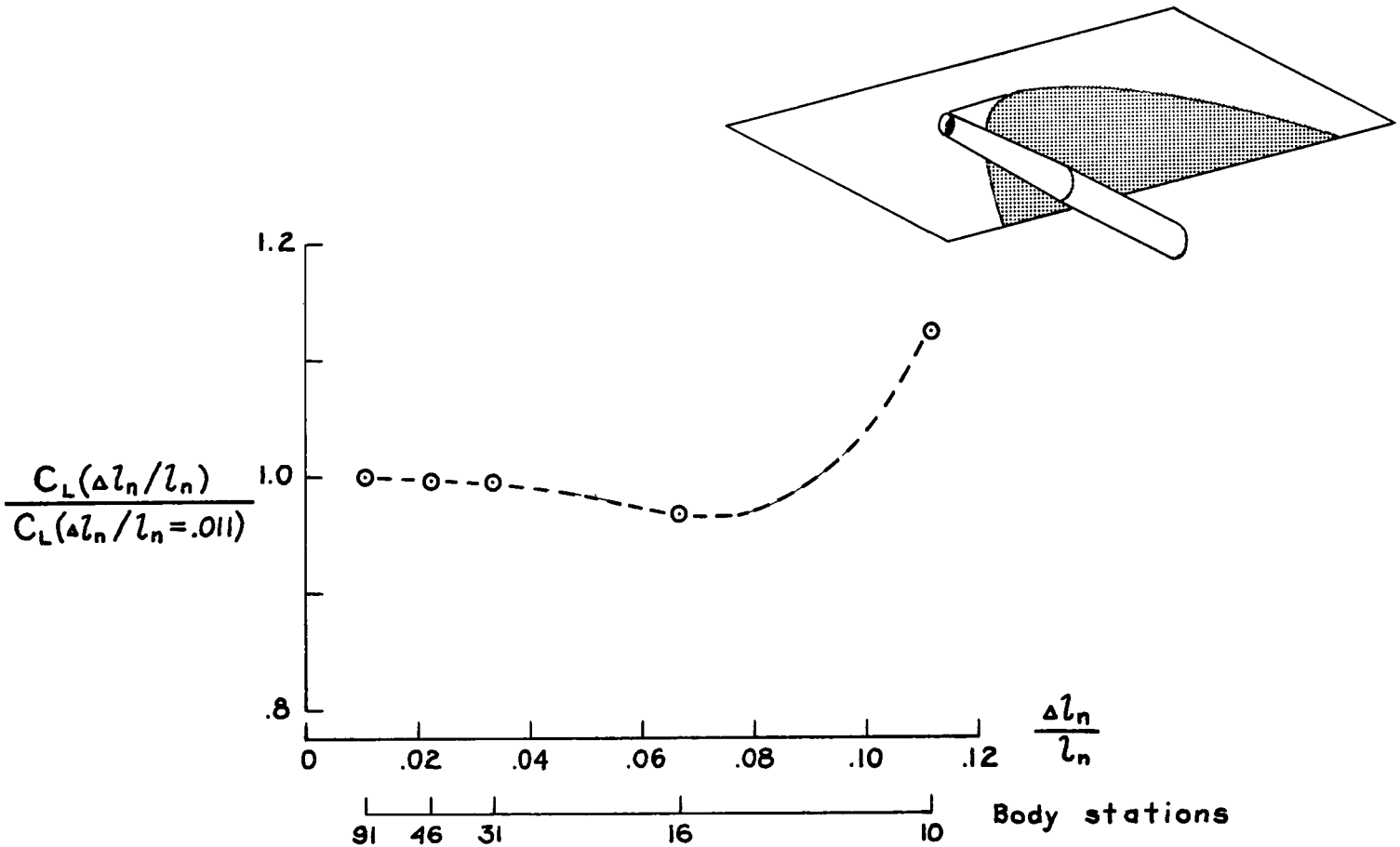

(b) N_{max} = 50, M = 2.0.

Figure 6.- Concluded.

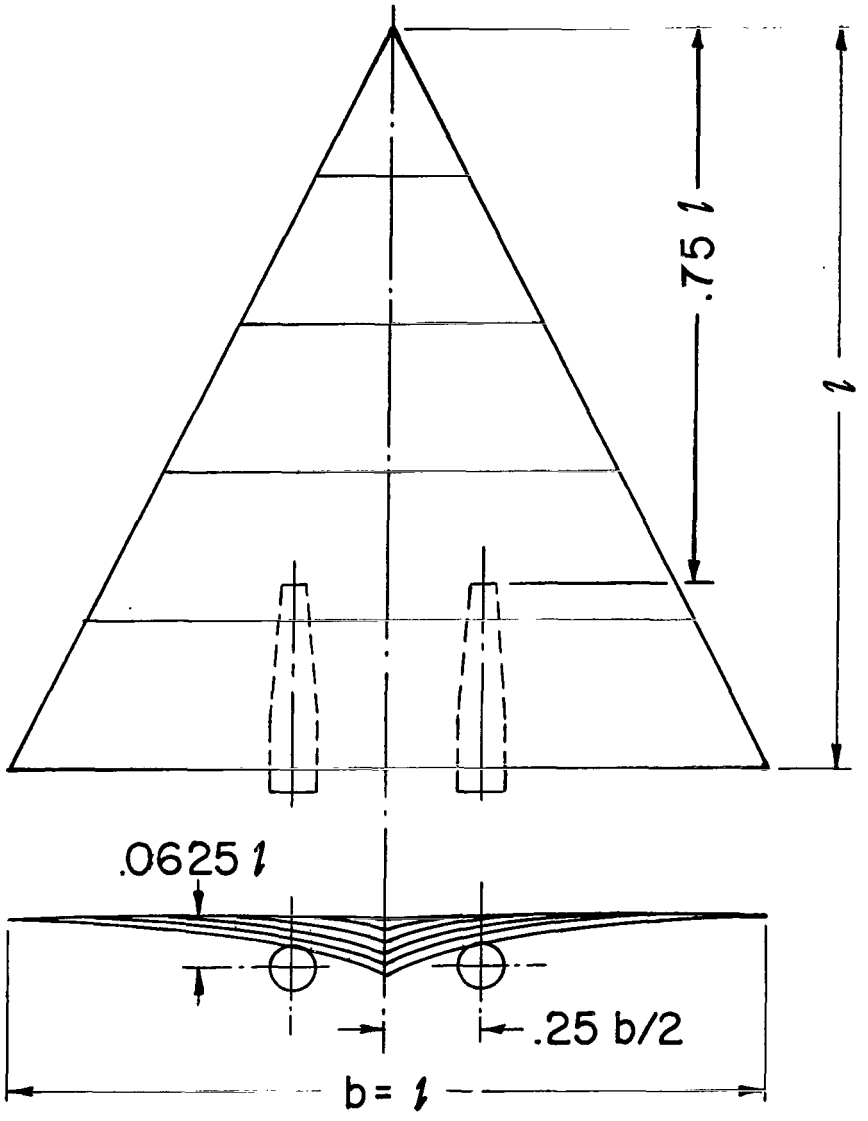

Figure 7.- Sketch of example twisted and cambered wing-nacelle combination.

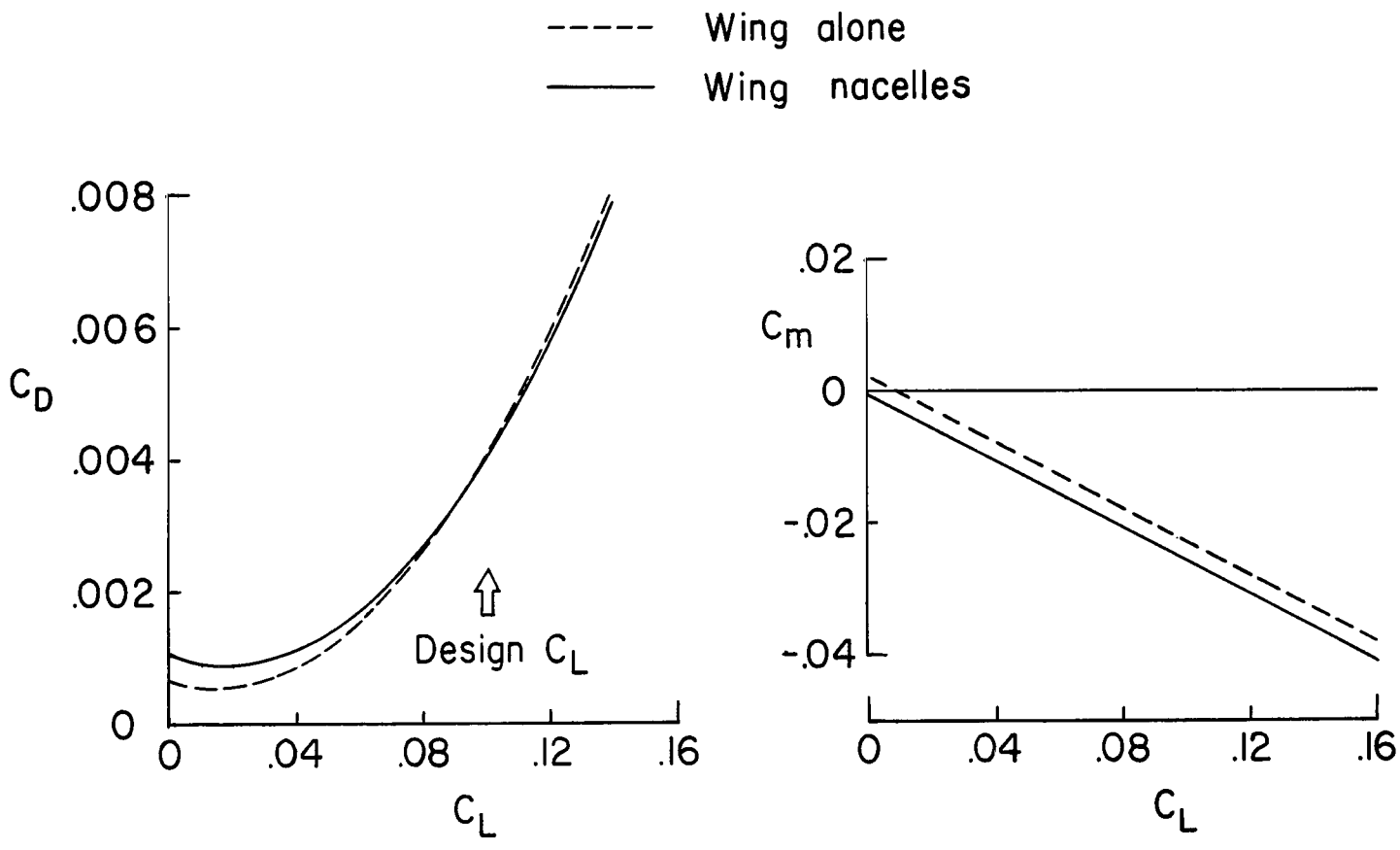

Figure 8.- Aerodynamic characteristics of twisted and cambered wing-nacelle combination for 0-percent reflex.

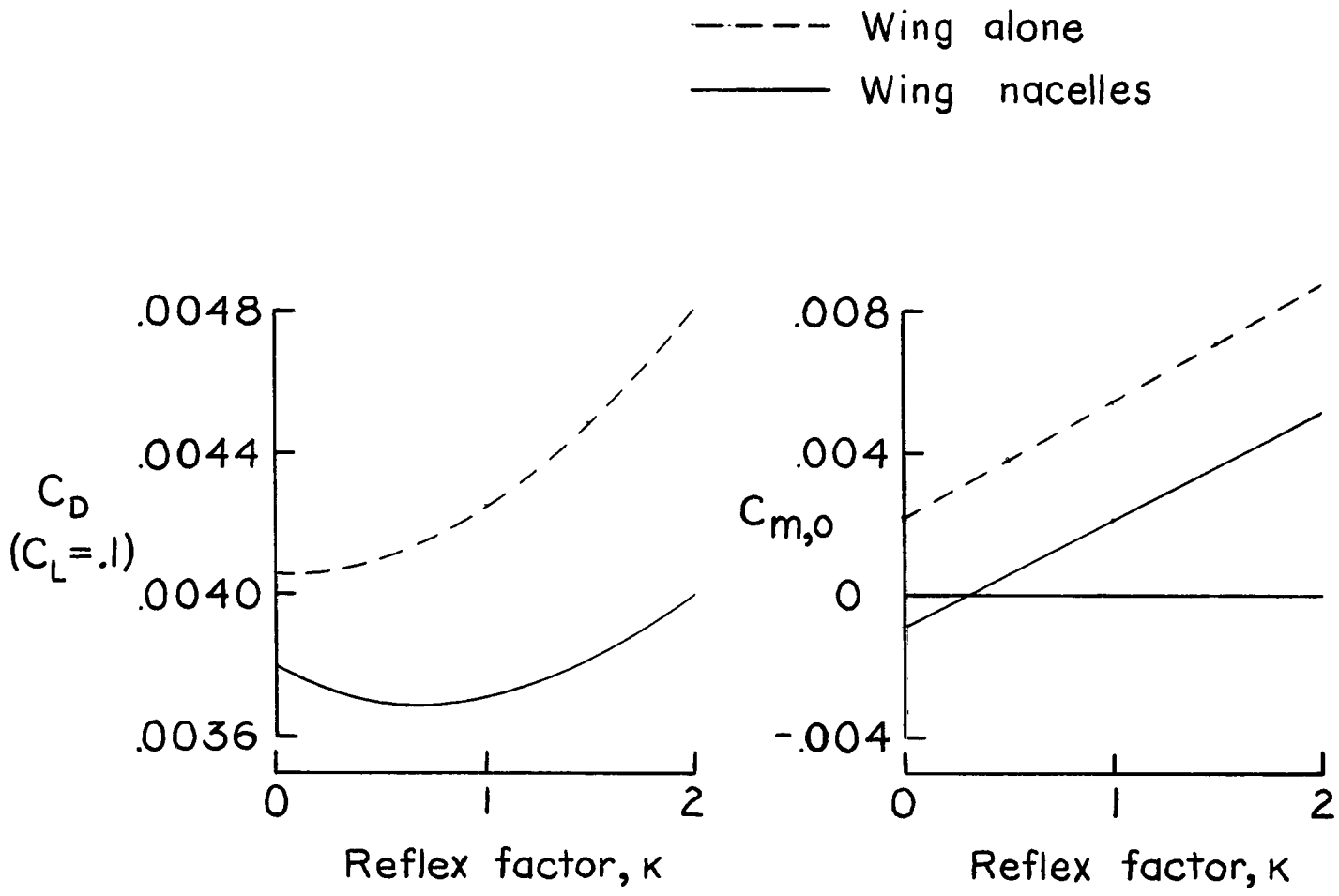

Figure 9.- Effect of reflexing on aerodynamic characteristics of twisted and cambered wing-nacelle combination.

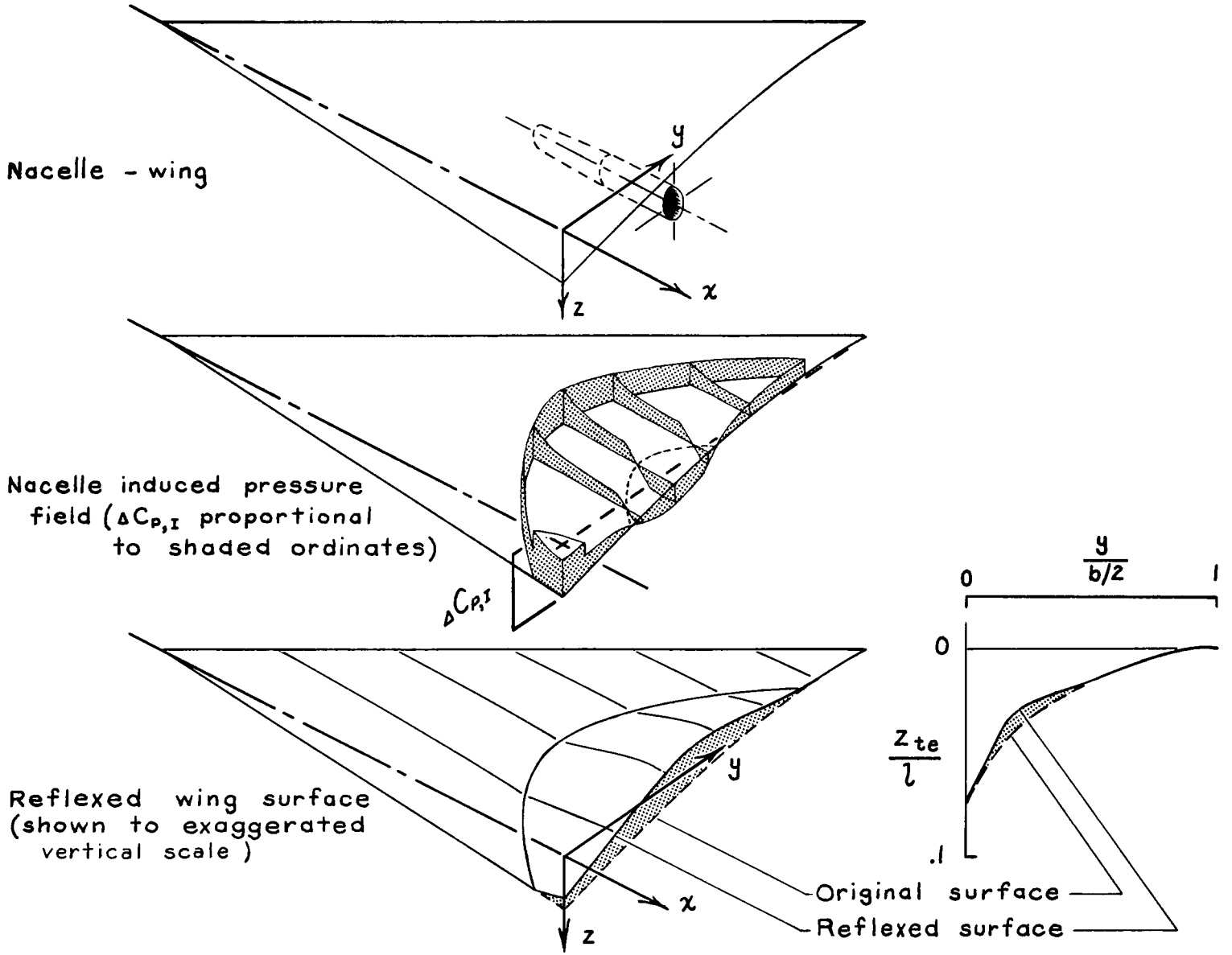

Figure 10.- Nacelle pressure field at surface of twisted and cambered wing and reflex surface required for 100-percent cancellation.

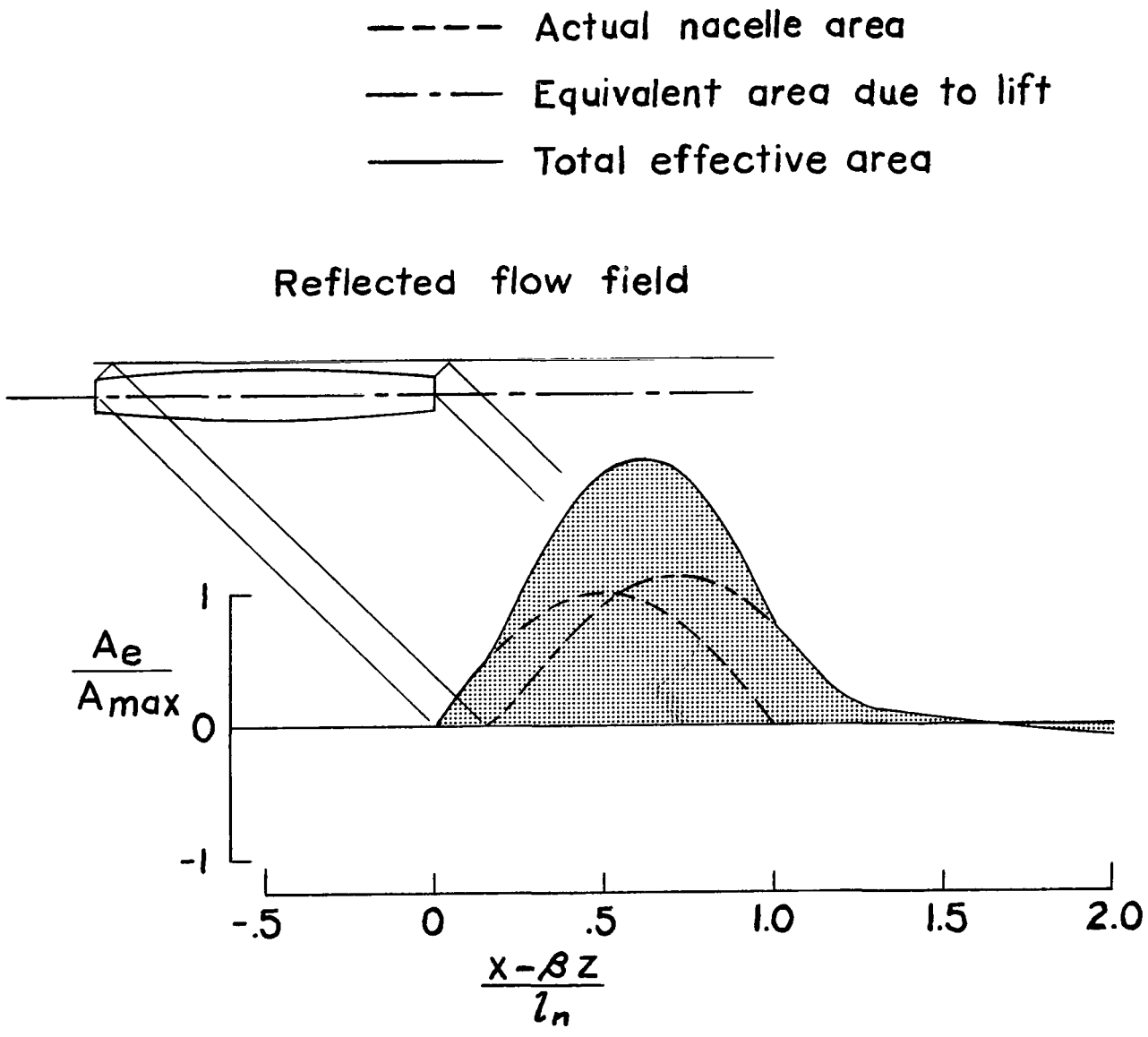

Figure 11.- Example of development of nacelle effective area distributions for use in sonic-boom calculations.

NASA-Langley, 1969 — 1 L-5691

NATIONAL AERONAUTICS AND SPACE ADMINISTRATION
WASHINGTON, D. C. 20546

OFFICIAL BUSINESS

FIRST CLASS MAIL

POSTAGE AND FEES PAID
NATIONAL AERONAUTICS AND
SPACE ADMINISTRATION

"The aeronautical and space activities of the United States shall be conducted so as to contribute . . . to the expansion of human knowledge of phenomena in the atmosphere and space. The Administration shall provide for the widest practicable and appropriate dissemination of information concerning its activities and the results thereof."

—NATIONAL AERONAUTICS AND SPACE ACT OF 1958

NASA SCIENTIFIC AND TECHNICAL PUBLICATIONS

TECHNICAL REPORTS: Scientific and technical information considered important, complete, and a lasting contribution to existing knowledge.

TECHNICAL NOTES: Information less broad in scope but nevertheless of importance as a contribution to existing knowledge.

TECHNICAL MEMORANDUMS: Information receiving limited distribution because of preliminary data, security classification, or other reasons.

CONTRACTOR REPORTS: Scientific and technical information generated under a NASA contract or grant and considered an important contribution to existing knowledge.

TECHNICAL TRANSLATIONS: Information published in a foreign language considered to merit NASA distribution in English.

SPECIAL PUBLICATIONS: Information derived from or of value to NASA activities. Publications include conference proceedings, monographs, data compilations, handbooks, sourcebooks, and special bibliographies.

TECHNOLOGY UTILIZATION PUBLICATIONS: Information on technology used by NASA that may be of particular interest in commercial and other non-aerospace applications. Publications include Tech Briefs, Technology Utilization Reports and Notes, and Technology Surveys.

Details on the availability of these publications may be obtained from:

SCIENTIFIC AND TECHNICAL INFORMATION DIVISION

NATIONAL AERONAUTICS AND SPACE ADMINISTRATION

Washington, D.C. 20546